Indian Journal of Chemical Technology
Vol. 22, May-July 2015, pp. 95-104

CFD simulations of immobilized-titanium dioxide based annular photocatalytic reactor: Model development and experimental validation

Jatinder Kumar* & Ajay Bansal

Department of Chemical Engineering, Dr B R Ambedkar National Institute of Technology, Jalandhar 144 011, Punjab, India

E-mail: jkumar.nitj@gmail.com

Received 17 September 2013; accepted 6 March 2014

A CFD (Computational fluid dynamics) model for predicting the performance of an immobilized-titanium dioxide based annular photocatalytic reactor has been developed. The CFD model is based on the intrinsic kinetic parameters determined experimentally in a perfectly mixed batch reactor. Experiments are also performed using an actual immobilized-titanium dioxide based annular photocatalytic reactor to obtain the experimental results. The modeling predictions are compared with the experimental results for validation of the CFD model. The modeling predictions agree closely with the experimental data. It is observed that CFD could become a valuable tool to understand and improve the photocatalytic systems.

Keywords: Computational fluid dynamics (CFD), Photocatalysis, Titanium dioxide, Photocatalytic reactor, Simulation, Water treatment.

Photocatalysis is a promising and emerging method of water purification as the process occurs at room temperature and pressure[1-3]. Photocatalysis is able to oxidize low-concentration pollutants to water, carbon dioxide, and harmless compounds[4]. Photocatalytic processes involve the use of nanostructured photocatalyst materials in the presence of ultraviolet radiations for oxidation reactions. Titanium dioxide (TiO_2) is the most widely used photocatalyst because it is chemically inert, environmentally friendly, economical, and highly stable. It is easy to use, and able to efficiently catalyze reactions[5]. Although extensive laboratory research has been done in the field of heterogeneous photocatalysis, there are several challenges preventing the development of this technology to the commercial scale. It is a complicated task to model, simulate, design, optimize, and scale-up a photocatalytic reactor as it involves simultaneous processes of fluid flow, momentum transfer, mass transfer, reaction kinetics, and radiation distribution. A dearth of modeling and simulation strategies for evaluating such complex systems, and lack of adequate scale-up methods is a huge restriction in the commercialization of photocatalytic reactors.

Modeling and simulation of photocatalytic reactors require simultaneous solution of momentum and mass-transfer equations, radiation transfer equation, and heterogeneous photocatalytic reaction kinetics[6]. The solution of this set of equations might be a tough challenge, not only due to mathematical complexity but also because of their strong coupling. As a result, in many of the models reported in literature, simplifying assumptions in one or more of these equations have been made to simplify the mathematical solution. However, the solution of the governing equations under simplification assumptions limits the applicability of the model to simple systems where those conditions apply. In order to properly predict the behavior of a photoreactor under different operating conditions, a rigorous solution of the governing equations of the system is desired. Many photocatalytic systems have been reported in literature, such as the fixed bed reactor[7,8], fluidized bed reactor[9,10], honeycomb monolith reactor[11,12], titanium dioxide coated fibre-optic cable reactor[13], annular reactor[14] and annular venturi reactor[15]. However, other than a few exceptions, reactor design has largely been based on empirical considerations, rather than first principles. Recently, first principles based CFD has extensively been demonstrated to be a very effective tool for the simulation of reacting system[16], and this technique has been extended for modeling of photocatalytic systems.

With the increased performance of computational resources, and development of simulation software,

CFD is becoming an affordable engineering tool to simulate and optimize reactor designs. While CFD is being developed as a mainstream modeling tool, anticipating flow characteristics, and selecting the appropriate modeling technologies (boundary conditions, flow model, type of solver etc.) remain the responsibility of the user. CFD solves the governing equations of flow, mass, and momentum conservation in the discretized computational domain using a numerical (e.g. finite volume) method. As CFD is based on the governing equations of mass and moment conservation, there are many possible sources for error, and validation of the CFD results is very important for the use of such a model[17]. Among the factors that may influence the CFD results are the discretisation of the domain (structure and size of the cells) and type of the modeling approach employed (physical flow model and solver etc.). Grid generation is one of the most important parts of CFD analysis. The quality of grid has a direct influence on the quality of the analysis, regardless of the flow solver used. Additionally, the solver will be more robust and efficient when using a well-constructed mesh. A quality grid capable of representing the geometry is the basis for a reliable and accurate simulation. In general, both mesh quality, and grid independence of the solution need to be ensured[18].

The application of CFD in reaction engineering is well known, and has been applied in many areas of chemical engineering and chemical reaction engineering[19], such as fluidization[20-22], multiphase flow systems[23-26], and more recently it has been utilized for simulation of immobilized-titanium dioxide based photocatalytic reactor[19,27-33].

In all of the previous CFD studies involving immobilized-titanium dioxide based photocatalytic reactor, nothing has been mentioned about the immobilization technique utilized for attaching nano-particles of titanium dioxide to the support, and criteria for selection of a particular immobilization technique. The method of immobilization has a great effect on the kinetics of a photocatalytic reaction, and hence, on the modeling, design, scale-up and commercialization of a photocatalytic reactor. Also, a little information is provided, in the earlier studies, about the sensitivity of a solution of a CFD model to the size of the grid (mesh) in the physical domain of the reactor. Mesh independence of the CFD results is an imperative part of any CFD analysis, and required for efficient simulation of the system. Above all, almost all the previous studies available in literature on immobilized-TiO_2 based annular photocatalytic reactor have been carried out for air treatment. In case of water treatment, research work is inadequate as far as immobilized-TiO_2 based annular photocatalytic reactor is concerned. More recently, the authors of the present work studied the hydrodynamics and mass transfer of Rhodamine B in an annular reactor for an aqueous solution using CFD, and results of the investigation has been published elsewhere[34]. There was no photocatalytic reaction involved, and the study was limited to only two crucial issues of annular reactor; hydrodynamics and mass transfer.

The current investigation aims to reduce the research gaps, present in literature, mentioned in the previous paragraph. The study deals with development, and experimental evaluation of a CFD model for immobilized-TiO_2 based annular photocatalytic reactor for water treatment. The computational model integrates hydrodynamics, species mass transport, and chemical reaction kinetics using a commercial CFD code Fluent 6.3.26. The model is based on intrinsic chemical parameters determined experimentally in the perfectly mixed batch reactor. An immobilization technique has been selected based on the photocatlytic performance, and the selected technique was utilized for immobilization of titanium dioxide on the surface of the photoreactor. The immobilized titanium dioxide has been characterized using XRD (X-ray diffraction) and SEM (Scanning electron microscopy) to analyze the photocatalytic properties of the titanium dioxide after immobilization. Rhodamine B, a complex organic compound, was selected as a test pollutant. It is an organic dye, and highly soluble in water.

Methodology

CFD modeling and computational details

Transport equations and kinetics

In present study, it is assumed that the fluid is newtonian, incompressible and isothermal with constant physical properties. The transport and chemical reaction were modeled by solving mass, momentum and species conservation equations using commercial CFD code Fluent 6.3.26 (Fluent Inc., USA). The simulation of the system was performed with a three-dimensional, steady state, laminar-flow model including the photocatalytic surface reaction. Detailed description of the conservation equations along with the associated correlations and parameters are provided in the Fluent Manual[35].

In the present work, reaction involved was heterogeneous photocatalytic degradation of Rhodamine B over immobilized-titanium dioxide. The overall reaction was treated as surface reaction leading to complete mineralization of Rhodamine B ($C_{28}H_{31}ClN_2O_3$):

$$C_{28}H_{31}ClN_2O_3 + 36\frac{1}{2}O_2 \xrightarrow{TiO_2} 28CO_2 + 2HNO_3 + HCl + 14H_2O \quad \ldots(1)$$

Under the experimental conditions used in this study, the surface photocatlytic decomposition of Rhodamine B followed pseudo first-order kinetics with respect to the concentration of of Rhodamine B at constant UV irradiance according to the Langmuir-Hinshelwood kinetics. The overall rate expression, R_{RB}^S for photocatalytic degradation of Rhodamine B was defined by:

$$R_{RB}^S = kM_{w,RB}[C_{28}H_{31}ClN_2O_3] \quad \ldots(2)$$

and alternatively,

$$R_{RB}^S = kC_{RB}^S \quad \ldots(3)$$

where $M_{w,RB}$ is the molecular weight of Rhodamine B, $[C_{28}H_{31}ClN_2O_3]$ and C_{RB}^S is the molar and mass concentrations of Rhodamine B at the catalyst surface, respectively, and k is the surface reaction rate constant. The laminar finite rate model, in which the transport equations are solved for species mass fraction with the predefined chemical reaction mechanism, was chosen for reaction modeling. This model ignores the effects of turbulent fluctuations on reaction rate. Models of this type are suitable for simulating a broad range of reacting system.

Geometrical model and grid generation

The annular reactor geometry studied in the present research is shown in Fig. 1(a). The reactor consists of 38 mm outer tube diameter, 27 mm inner tube diameter, and 500 mm total length with 12 mm diameter inlet and outlet tubes. The inlet and outlet tubes were placed at the two extreme ends of the reactor to form a U-shape annular reactor. The 450 mm middle length on the inner wall of the outer tube was used to set up photocatalytic surface reaction in CFD model because this length of the annular reactor

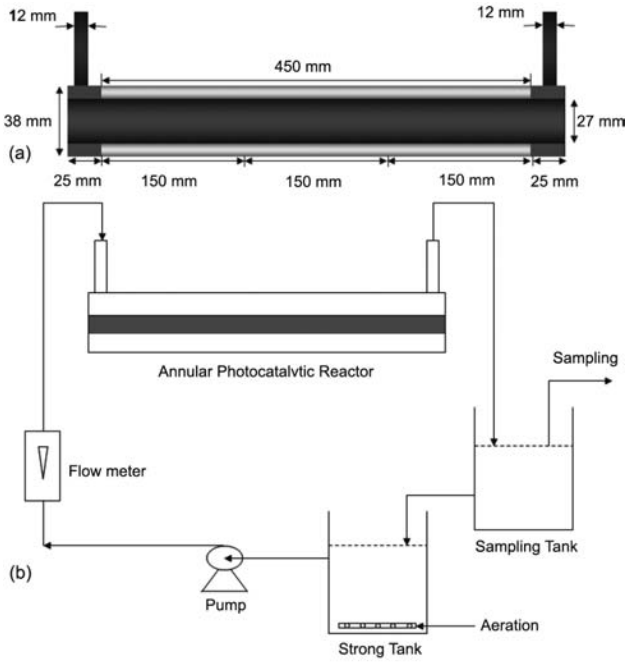

Fig. 1 — (a) Schematic diagram of annular reactor, (b) Experimental setup for photocatalytic degradation in annular reactor

was coated with titanium dioxide in actual experiments. The commercial software Gambit 2.2.16 was utilized to create geometry and grid for CFD modeling. The cooper meshing technique was used to generate the grid in present case. The hexahedral cells were used to discretize the reactor domain where the photocatalytic surface reaction was to be studied (middle annular region of length 450 mm). The unstructured cells were used in other part of the reactor geometry.

To test the grid independence of the CFD solution, five computational grids were considered in the discretization of the reactor geometry. Five mesh sizes were having different number of cell volumes; mesh-1 (53703 cells), mesh-2 (158874), mesh-3 (790818), mesh-4(1219830), and mesh-5 (1876688). The axial velocity in the annular region, and area-weighted average mass fraction of Rhodamine B at the outlet of the reactor was used as criterion for judging the grid independence of the CFD results.

Boundary conditions and physical properties

The boundary conditions for the CFD model were defined as follows. At the inlet, velocity of the fluid was specified. Two flow velocities 9.08×10^{-3} m/s and 4.54×10^{-2} m/s corresponding to Reynolds

number of 20 and 100, respectively, were chosen for CFD analysis. The direction of the flow was defined normal to the boundary. The inlet mass fraction of Rhodamine B was specified as 1×10^{-5} which corresponds to 10 ppm concentration of Rhodamine B in the solution. At the outlet, boundary condition pressure-outlet was specified with a value of 1 atm. At all the walls, a no-slip boundary condition was imposed. Also, zero diffusive flux of species was specified at the walls, except for the wall (middle length of 450 mm of the inner surface of the outer pipe of annular reactor) where the photocatalytic surface reaction of degradation of Rhodamine B was specified. At this wall surface, the boundary condition was defined according to the rate equation. The physiochemical process studied in this investigation is the degradation of Rhodamine B in water at room temperature. The concentration of Rhodamine B used in present work was very low (10 ppm), so the physical properties of water were assumed for the solution. The density and viscosity of water considered were 998.2 kg/m^3 and 10.03×10^{-4} Pa.s, respectively.

CFD solution strategy

Commercial CFD code Fluent 6.3.26 was used to perform simulations. The governing equations were solved using pressure based three dimensional solver. Second order upwind discretization scheme was employed except for pressure. PRESTO was selected as discretization scheme for pressure. The SIMPLE algorithm was chosen for the pressure-velocity coupling. The default values of under-relaxation factors were considered. Convergence of numerical solution was ensured by monitoring the scaled residuals to a criterion of 10^{-4} for the continuity and momentum variables, and 10^{-6} for the concentration. The solution of the model was utilized to find out the concentration field, conversion yield, degradation profile, and reaction rate constant.

Experimental Section

Materials

Degussa P25 (TiO_2) catalyst provided by Evonik Industries, Germany was used throughout the current investigation without further modification. According to manufacturer's specifications, its BET surface area was 55 ± 15 m^2/g, average particle size was around 30 nm, purity was 97%, and anatase to rutile ratio was 80:20. Rhodamine B ($C_{28}H_{31}ClN_2O_3$) was procured from s d Fine Chemical Ltd, Mumbai, India. The water used was prepared in laboratory by double distillation processes. The annular and batch photocatalytic reactors were manufactured at Vijay Axiom, Ambala, India.

Catalyst immobilization and characterization

The catalyst (TiO_2) was immobilized on the desired surfaces using heat treatment technique according to the process mentioned by Khataee *et al.*[36]. The selection of this immobilized technique was based on a comparative study of three immobilization techniques *viz* heat treatment technique[36], acrylic binder method[37], and polyvinyl-formaldehyde method[38]. The criterion for comparison was the photocatalytic performance of the immobilized titanium dioxide in a photocatalytic activity test. The experimental set-up and methodology adopted for the photocatalytic activity test has been published by authors elsewhere[39].

The morphology of the immobilized titanium dioxide was studied using scanning electron microscopy (SEM). The sample was coated with gold before analyzing in scanning electron microscope JSM 6100 (Jeol) operated at 25 kV. The X-ray diffraction (XRD) analysis of immobilized titanium dioxide was done by plate XRD technique to study the crystalline structure. The XRD pattern was obtained on a Phillips PW-1710 X-ray diffractometer using Cu Kα radiation as X-ray source at an angle of 2θ ranging from 20° to 80°. The measurement was carried out at a scanning rate of 0.034 (2θ)/s.

Intrinsic reaction kinetics

The intrinsic kinetics of photocatalytic degradation of Rhodamine B was determined in a perfectly mixed batch photocatalytic reactor using the immobilized titanium dioxide. The batch reactor was consisted of 59 × 28.5 × 56 cm rectangular reaction chamber with interior covered with aluminum foil. Two 15-W, low pressure mercury vapour discharge UV lamps (F15T8/GL, Phillips) were positioned horizontally on the top of two opposite sides of the cabinet interior. Temperature probe was fixed in the chamber to record the chamber temperature. A small rotary fan was connected in the chamber for maintaining the temperature, and cooling the lamps. A working area of 38.5 × 19 cm was available in the chamber for the experiments. The experiments were carried out for 70 ml of sample solution each time in batch wise. Initial concentration of Rhodamine B in the sample was kept

as 10 ppm. The dye solution was poured into a beaker having bottom surface cross sectional area of 70.9 cm^2. Titanium dioxide was immobilized on the bottom surface of the beaker in such a way that a circular area of 18.1 cm^2 at the center was blank without the coating. The blank area was utilized for magnetic stirring during the experiments. The beaker was placed onto the working area of the photocatalytic reactor. Two UV light sources were then switched on, and the solution was irradiated with the ultraviolet light. The incident light intensity on the catalyst surface was kept at 6.1 mW/cm^2 by adjusting the vertical position of the UV lamps. This light intensity (6.1 mW/cm^2) was the same as used in the photocatalytic degradation studies in annular photocatalytic reactor. The cooling fan was also switched on in order to maintain the temperature of the photocatalytic chamber. The concentration of the Rhodamine B at different reaction time was determined by measuring the absorbance intensity at λ_{max} = 554 nm with the help of the UV-Vis spectrophotometer. The experiments were performed at various rotations per minute (rpm) of the magnetic stirrer to find out the intrinsic reaction rate constant without the mass transfer limitations.

Photocatalytic degradation in annular reactor

The CFD modeling and simulation was evaluated against the experimental performance of immobilized-titanium dioxide based annular photocatalytic reactor. The actual reactor had the same structure and dimensions as the geometrical model described in Fig. 1(a) used for CFD simulations. Total length of the reactor was 500 mm out of which middle 450 mm of the length was utilized for photocatalytic degradation of Rhodamine B. Titanium dioxide was immobilized on the inner surface of the outer tube in such a way to form 450 mm reactor length coated with titanium dioxide in the middle region of the reactor as shown in Fig. 1(a). Titanium dioxide was immobilized according to the already mentioned techniques. The outer glass tube of the reactor was having an inner diameter of 38 mm while the inner quartz tube was of 27 mm outer diameter. A low pressure mercury vapour discharge UV lamp (F15T8/GL, Phillips), a source of UV radiation, was housed within the inner tube of the reactor. The inner tube was made of quartz so as to allow maximum passage of UV light through it to the reacting fluid. The desired length (450 mm) of the UV lamp was obtained by covering both ends of the lamp with teflon tape. The immobilized-titanium dioxide based annular photocatalytic reactor was operated in recirculating batch mode using an experimental setup similar to the one shown schematically in Fig. 1 (b). In this experimental setup, the capacity of storage and sampling tank was 2 L. The sampling was performed with the help of a syringe. The storage tank was equipped with an aeration system required for agitation as well as mixing of ambient oxygen for better results. The operation of the system involved recirculation of 1000 mL of aqueous solution of Rhodamine B. The peristaltic pump (RH-P120S) was used for maintaining the flow through the system. The system was operated at flow rates of 62 mL/min and 308 mL/min corresponding to Reynolds number of 20 and 100, respectively. The initial concentration of Rhodamine B in aqueous solution was 10 ppm which is the same as used in CFD simulations. The photocatalytic degradation study in annular reactor was performed for 240 min in each case. The sampling was done at every 30 min to measure the concentration of Rhodamine B in the reacting fluid.

Results and Discussion

Grid Independence

The primary objective of this part of the study was to evaluate the size of computational grid required to obtain the grid independent results of the CFD model. A grid refinement process was undertaken by gradually increasing the number of cell volumes (mesh size) in the computational domain, and observing its effect on the outcome of the simulation. Five mesh sizes were utilized to see the dependency of axial velocity and area-weighted average mass fraction of Rhodamine B on the mesh size (number of cell volumes). The CFD model utilized was the same as discussed in Geometrical model and grid generation section, and the Reynolds number for the flow was 20. It is shown in Fig. 2 that there is a little difference in axial velocity profiles for mesh-3 (790818 cell volumes) and mesh-4 (1219830 cell volumes). Almost no difference in the axial velocity profiles of annular region was observed for mesh-4 (1219830 cell volumes) and mesh-5 (1878688 cell volumes). It means the refinement of grid from mesh-4 to mesh-5 does not bring any change in the axial velocity, and hence the results, in terms of axial velocity in annular region, obtained using mesh-4 are grid independent. Similarly, area-weighted average mass fraction of Rhodamine B at the outlet after the

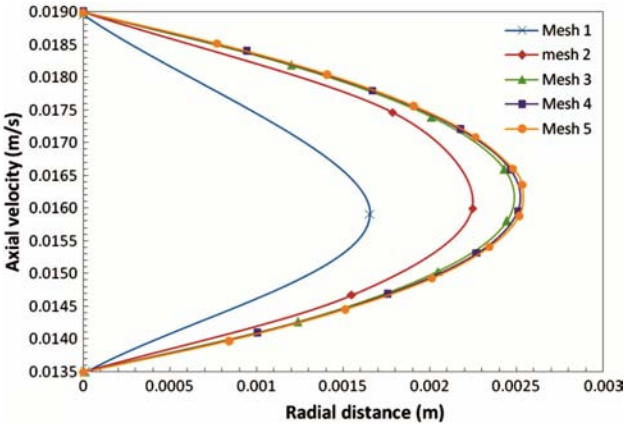

Fig. 2 — Axial velocity profiles for different mesh sizes

first pass was simulated for the five mesh sizes. The relative error between the mass fraction obtained for mesh-4 and mesh-5 is 0.02 %. It is obvious that the mass fraction obtained using mesh-4 is independent of further increase in mesh size. Thus, increasing the mesh size from mesh-4 to mesh-5 has no effect on the results produced in both the cases of axial velocity and mass fraction. The outcome of the CFD model using mesh-4 (1219830 cell volumes) is grid independent, and used further in CFD simulation of annular photocatalytic reactor.

Catalyst immobilization and characterization

The photocatalytic performance of the titanium dioxide immobilized by three different techniques was compared in terms of half-life time and rate constant. A detailed discussion regarding the same has been presented elsewhere[39]. It was observed that the titanium dioxide immobilized by heat treatment technique showed better photocatalytic performance in the photoactivity test. Therefore, heat treatment technique[37] was further utilized in the present study for immobilizing titanium dioxide on the surface of actual annular photocatalytic reactor.

To study the morphology, SEM image of the immobilized titanium dioxide was taken at ×10000 magnifications, and shown in Fig. 3. It is obvious from the micrograph that TiO_2 (white spots) is almost uniformly distributed on the surface. The SEM image also demonstrates the nanostructure of the catalyst, and rough surface of the film, which is quite necessary for good photocatalytic activity of the immobilized particles.

The XRD studies were made to notice any change in the phase composition and photocatalytic properties

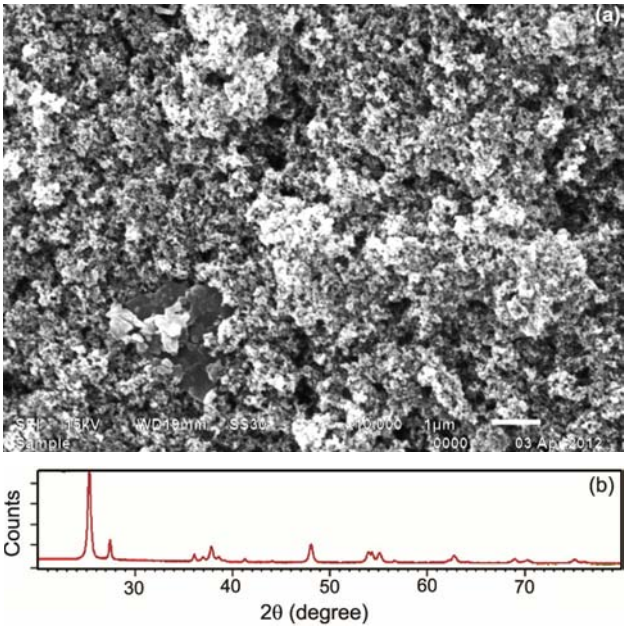

Fig. 3 — (a) SEM image (b) XRD pattern of immobilized titanium dioxide

of the titanium dioxide after immobilization on the support. The XRD pattern of the immobilized titania did not show any variation of the structure and phase composition due to immobilization process. The diffraction peaks observed at 2θ = 25.28°, 37.8°, 48.05°, 53.89°, 55.06°, and 62.69° correspond to the known diffraction maxima of anatase phase of titanium dioxide. The peaks at 2θ = 27.46°, 36.1°, 41.66°, 54.34°, and 56.6° correspond to rutile phase of titania. The intensity of the peaks reveals that the major phase available in the immobilized titania is anatase while the rutile is the minor phase. The anatase phase is supposed to be the most active one for the photocatalytic reactions.

Intrinsic reaction kinetics

In order to minimize the number of experiments and calculations, intrinsic photocatalytic oxidation kinetics was determined in a perfectly mixed batch photoreactor using the same catalyst (immobilized titanium dioxide), pollutant (Rhodamine B), and UV light irradiance (6.1 $mWcm^{-1}$) as used in the annular photocatalytic reactor. Theoretically, the reaction rate is determined by adsorbed irradiance. Since, the absorbed irradiance is difficult to determine with accuracy, reaction rate was determined on the basis of incident irradiance. One can reasonably assume that for a given catalyst, the ratio of the incident irradiance and absorbed irradiance is the same whatever the

photoreactor[32]. In the present intrinsic kinetics study, the dependence of reaction kinetics on incident irradiance has not been evaluated as the experiments were carried out at same irradiance as in the case of annular photocatalytic reactor. For determining the intrinsic kinetics of the immobilized photocatalytic reaction, it is necessary to make sure that the reaction is not affected by mass transfer limitation. So, several experimental runs using different rpm (rotations per minute) of magnetic stirrer were made to find the proper operating conditions of the batch photocatalytic reactor for determining intrinsic parameters of the reaction. The experimental observations and collected data were fitted according to Langmuir-Hinshelwood law of pseudo-first order photocatalytic reactions, and intrinsic parameters were then determined using the relationship:

$$r = \frac{dC}{dt} = \frac{\mathrm{k}KC_o}{1 + KC_o} \qquad \ldots(4)$$

where K represents the adsorption equilibrium constant on the surface, k is proportionality constant which provides a measure of the intrinsic reactivity of the photoactivated surface with pollutant, and C_o is the initial concentration of the pollutant. At very small concentrations, Eq. (4) is reduced to a simple first order rate expression. The term kK is referred as rate constant (k) or pseudo-first order rate constant. The increase in rate constant with respect to rpm (rotations per minute) was observed due to the presence of mass transfer limitation in the photocatalytic reaction till 500 rpm. As the rpm is increased from 500 to 600, no increase in the rate constant was observed indicating no effect of mass transfer on the reaction rate. The rate constant 0.1 min^{-1} (equivalent to 1.58×10^{-5} m/s based on surface area) calculated at 500 rpm represented the intrinsic rate constant of the photocatalytic reaction. The intrinsic rate constant is only related to the catalyst used (immobilized titanium dioxide) and the considered pollutant (Rhodamine B). It is independent of the reactor geometry, fluid dynamics and mass transfer. The intrinsic rate constant determined in a given reactor geometry can be used in other reactor configuration to evaluate the performance. Consequently, the calculated intrinsic rate constant was utilized in CFD simulation of annular photocatalytic reactor for validation of CFD modeling.

Photocatalytic degradation in annular reactor: CFD simulations and experimental results

The actual immobilized-titanium dioxide based annular photocatalytic reactor was operated in laboratory in recirculating batch mode to analyze the performance. The reactor was operated at different Reynolds numbers (Re = 20 and 100), and performance of the reactor was measured in terms of degradation rate as shown in Fig. 4. The error bars represent the standard deviation obtained with triplicate runs. The data was best fitted by Langmuir-Hinshelwood kinetic model in accordance with the literature[19,31,39]. The CFD simulations were performed for the same reactor under the exact operating conditions as of the laboratory experiments. The outcome of the CFD simulations is also represented in Fig. 4. The CFD predictions and the experimental results for decrease in concentration of Rhodamine B with respect to time in the annular photocatalytic reactor are compared in Fig. 4(a). For two different flow rates (Re = 20 and 100), the CFD model provides close agreement with experimental data in predicting the exponential decrease in concentration

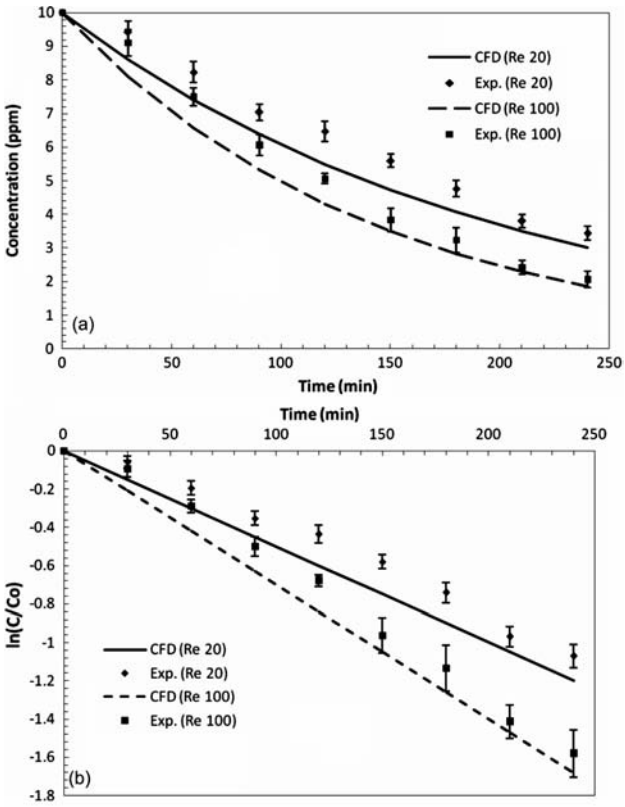

Fig. 4 — Photocatalytic degradation in annular reactor at Re = 20 and Re = 100 (a) Time effect on degradation of Rhodamine B, (b) Kinetics of degradation

of Rhodamine B. The reaction rate constants for different flow conditions were determined by representing the obtained data as shown in Fig. 4 (b). The slope of the best fitted straight line to the experimental as well as simulated data was utilized to calculate the reaction rate constants. The simulated value of the reaction rate constants for Reynolds number 20 and 100 was evaluated as 0.005 min^{-1} and 0.007 min^{-1}, respectively. The relative error in simulated results was reported to be 18 % in comparison to the experimental results. Hence, it can be inferred that CFD modeling can efficiently predict the behavior of photocatalytic degradation in annular reactor.

It has been observed in experimental study as well as CFD simulations that reaction rate increases with increase in Reynolds number (Re) which is in agreement with literature[29]. This increasing trend confirms that the photocatalytic degradation process was limited by mass transfer under the studied flow conditions. At low Reynolds number (Re 20), there is a limited degree of radial mixing leading to less mass transfer of Rhodamine B to the surface of the photocatalyst. The small mass transfer coefficient at lower flow rate prevents the reactant molecules to reach the photocatalyst for adsorption and subsequent degradation, resulting in low reaction rate constant (0.005 min^{-1}). At high Reynolds number (Re 100), the radial mixing is comparatively more resulting in increase in diffusion rate of the reactant to and from the photocatalyst surface. Thus, the reduced mass transfer limitations at high flow rate results in high reaction rate (0.007 min^{-1}).

One of the major advantages of CFD simulations is that it allows comprehensive analysis of the reactor performance by providing the local values of the parameters of interest which is not possible in the case of conventional empirical techniques. Taking a note of this advantage, the contours of molar concentration of Rhodamine B during the first pass of solution through annular photocatalytic reactor for Re = 20 and 100 were obtained using CFD simulations, and presented in Fig. 5. The contours correspond to the longitudinal center plane of the exit region of annular geometry. It is apparent from the contours of molar concentration that the concentration decreases along the photoreactor length as expected. Figure 5 also shows a comparison of contours of molar concentration of Rhodamine B for Reynolds number 20 and 100 during the first pass of reacting solution through the annular photocatalytic reactor. For the first pass, more decrease in concentration of Rhodamine B is observed in case of Re = 20 as compared to Re = 100 because at the low Reynolds number (Re = 20), the reacting stream has enough time to stay in the reactor for photocatalytic degradation. However, at high Reynolds number (Re = 100) because of comparatively high velocity, reactant has less time within the reactor to degrade photocatalytically. Figure 6 represents the cross-sectional view of contours of mass fraction of Rhodamine B at a distance 0.475 m from the inlet end

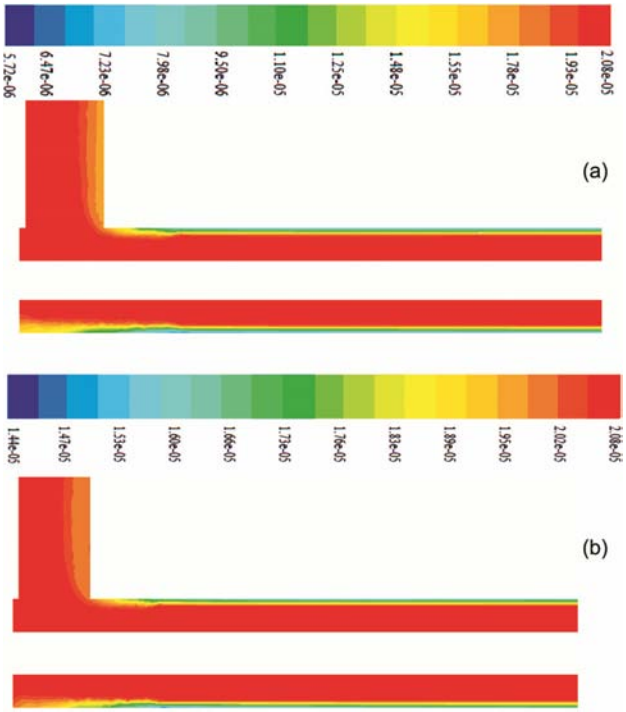

Fig. 5 — Contours of molar concentration (kmol/m^3) of Rhodamine B at exit (a) Re = 20 (b) Re = 100

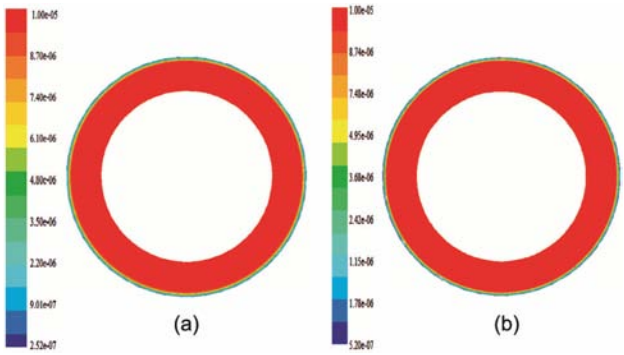

Fig. 6 — Contours of mass fraction of Rhodamine B at a distance 0.475 m from the inlet end of the photoreactor (a) Re = 20, (b) Re = 100

of the annular photoreactor for first pass of the solution for Re = 20 and 100. Both of the Figs. 5 and 6 depict that the radial concentration gradient exits in the annular region of the reactor with lower reactant concentration at the inner surface of the outer tube where the catlalyst (titanium dioxide) was immobilized. The lower concentration at the inner surface of the outer tube was expected as the photocatalytic degradation takes place only at the catalyst surface. The conventional empirical studies cannot provide means of visualization of concentration gradient in the photoreactor. CFD simulation has been capable of providing detailed information on the concentration of reactant at any given point along the reactor. Such information or any other detailed data from within the photocatalytic reactor, which can be obtained through CFD studies, is invaluable in understanding the process, and improving the photoreactor performance.

Conclusion

A CFD model for predicting the behaviour of an immobilized-titania based annular photocatalytic reactor has been developed. The results demonstrate close agreement between the modeling prediction and experimental data which indicates that CFD could become a valuable tool to understand and improve the photocatalytic reactors. The detailed local information of the simulated reactor (concentration profiles) is obtained using CFD which provided a qualitative understanding of the process to better explain the results. The concentration contours give an accurate insight to the photocatalytic reaction behaviour, and presented information which cannot be obtained from experiments. Hence, CFD approach can be extended for optimizing the performance and design of photocatalytic systems.

Acknowledgement

Authors express great sense of gratitude to Evonik Industries, Germany for providing titanium dioxide for the present research work.

Nomenclature

C_{RB}^{S} Mass concentration of Rhodamine B (ppm)

C_0 Initial concentration of Rhodamine (ppm)

$M_{w,RB}$ Molecular weight of Rhodamine B (kg kmol^{-1})

R_{RB}^{S} Surface rate of depletion of Rhodamine B (kg m^{-2} s^{-1})

K Adsorption equilibrium constant (ppm^{-1})

k Proportionality constant (ppm s^{-1})

k Pseudo-first order rate constant (s^{-1})

References

1 Ollis D F & Turchi C, *Environ Prog*, 9 (1990) 229.
2 Hoffmann M R, Martin S T, Choi W & Bahnemannt D W, *Chem Rev*, *95* (1995) 69.
3 Herrmann J, *Top Catal*, 34 (2005) 49.
4 Fujishima A, Rao T & Tryk D, *J Photochem Photobiol C*, 1 (2000) 1.
5 Carp O, Huisman C L & Reller A, *Prog Solid State Ch*, 32 (2004) 33.
6 Imoberdorf G E, Cassano A E, Alfano O M & Irazoqui H A, *AIChE J*, 52 (2006) 1814.
7 Peral J & Ollis D, *J Catal*, 136 (1992) 554.
8 Yoshikawa F, Namiki N, Otani Y & Biswas P, *J Chem Eng Jpn*, 37 (2004) 503.
9 Brucato A, Iatridis D, Rizzuti L & Yue P, *Can J Chem Eng*, 70 (1992) 1063.
10 Dibble L & Raupp G, *Environ Sci Technol*, 26 (1992) 492.
11 Sauer M & Ollis D, *J Catal*, 149 (1994) 81.
12 Hossain M, Raupp G, Hay S & Obee T, *AIChE J*, 45 (1999) 1309.
13 Peill N & Hoffmann M, *Environ Sci Technol*, 29 (1995) 2974.
14 Mohseni M & David A, *Appl Catal B Environ*, 46 (2003) 219.
15 Lasa H D & Ibrahim H, *US Patent 6752957*, (June 22 2004).
16 Kuipers JA & Swaaij WPV, *Adv Chem Eng*, 24 (1998) 227.
17 Sozzi D A & Taghipour F, *Int J Heat Fluid Fl*, 27 (2006) 1043.
18 Douglas R W, Carey G F, White D R, Hansen G A, Kallinderis Y & Weatherhil N P, *Numer Heat Transfer*, 41 (2002) 211.
19 Jarandehehei A & Visscher A D, *AIChE J*, 55 (2009) 312.
20 Grace J R & Taghipour F, *Powder Technol*, 139 (2004) 99.
21 Hoef M A V, Annaland M V & Kuipers J A M, *Chem Eng Sci*, 59 (2004) 5157.
22 Cooper S & Coronella C J, *Powder Technol,* 151 (2005) 27.
23 Jiang Y, Khadilkar M R, Dahhan M H A & Dudukovic A P, *AIChE J,* 48 (2002) 701.
24 Lamping S R, Zhang H, Allen B & Shamlou P A, *Chem Eng Sci*, 58 (2003) 747.
25 Kerdouss F, Bannari A & Proulx P, *Chem Eng Sci*, 61 (2006) 3313.
26 Taha T & Cui Z F, *Chem Eng Sci*, 61 (2006) 676.
27 Pareek V K, Cox S J, Brungs M P, Young B & Adesina A A, *Chem Eng Sci*, 58 (2008) 859.
28 Mohseni M & Taghipour F, *Chem Eng Sci*, 59 (2004) 1601.
29 Taghipour F & Mohseni M, *AlChE J*, 51 (2005) 3039.
30 Castrillon S R & Lasa H I D, *Ind Eng Chem Res*, 46 (2007) 5867.
31 Queffeulou A, Geron L, Archambeau C, Gall H L, Marquaire P & Zahraa O, *Ind Eng Chem Res*, 49 (2010) 6890.

32 Queffeulou A, Geron L & Schaer E, *Chem Eng Sci,* 65 (2010) 5067.

33 Vincent G, Schaer E, Marquaire P M & Zahraa O, *Process Saf Environ,* 89 (2011) 35.

34 Kumar J & Bansal A, *Heat Mass Transfer*, 48 (2012) 2069.

35 Lebanon N H, Fluent-Inc, *Fluent 63 User's Guide*, (2006).

36 Khataee A R, Pons M N & Zahraa O, *J Hazard Mater*, 168 (2009) 451.

37 Noorjahan M, Reddy M P, Kumari V D, Lavedrine B, Boule P & Subrahmanyam M, *J Photoch Photobio A*, 156 (2003) 179.

38 Kumar J & Bansal A, *Int J Environ Sci Technol*, 9 (2012) 479.

39 Kumar J & Bansal A, *Water Air Soil Pollut*, 224 (2013) 1452.